Ceramics International 44 (2018) 5901–5908

Contents lists available at ScienceDirect

Ceramics International

journal homepage: www.elsevier.com/locate/ceramint

Effect of Ag nanoparticles seeding on the properties of silica spheres

H. Misran[a,*], M.A. Salim[a], S. Ramesh[b,*]

[a] Nanoarchitectonic Laboratory, Department of Mechanical Engineering, College of Engineering, Universiti Tenaga Nasional, 43000 Kajang, Selangor, Malaysia
[b] Centre of Advanced Manufacturing & Material Processing, Department of Mechanical Engineering, Faculty of Engineering, University of Malaya, 50603 Kuala Lumpur, Malaysia

ARTICLE INFO

Keywords:
Silica
Ag-silica composites
Surface modification
Ag seeding

ABSTRACT

In this study, the effect of seed-recrystallization on the Ag deposition onto silica sphere surfaces has been investigated. It was found that increasing the seed-recrystallization cycles resulted in higher atomic deposition at ca. 84% coverage of silica surfaces with the same mole ratio of Ag precursor characterized by the Ag/Si atomic ratio obtained by XPS analyses. The addition of straight-chain palm oil derived fatty alcohols (PODFA) in the sol-gel prior to seed-recrystallization aided the deposition of Ag. Thus, PODFA play the role of nonsurfactant surface modification agent to produce Ag-silica nanocomposite. Structural analyses showed that the resulting Ag nanocrystallines having a face centre cubic structure and particle size of 5–20 nm were deposited homogeneously on silica spheres. Chemical state analyses from XPS indicated that the increasing number of seed repetition process increased the seeding of Ag nanoparticles on silica surface with the same molar of Ag atoms. XPS spectra at O1s orbital elucidated that the binding energy of three oxides components were determined at ca. 533.8 eV (Si-O-H), 532.8 eV (Si-O-Si) and 530.8 eV (Si-O-Ag), respectively. The high sensitivity of surface plasmon resonance observed in the nanocomposites prepared in this study are useful in optical applications.

1. Introduction

Surface coating of oxide nanoparticles and synthesis of hybrid composite material are continuously being studied to improve the materials with new and enhanced properties [1–3]. Sub-micrometer SiO_2 spheres exhibited high potential to be coated with functional metal nanoparticles due to their stability in physical and chemical properties, compatibility with other materials and easily accessible surface structure consisting of silanol groups (Si-OH) protruding from the surface. Si-OH were useful functional groups in surface coating procedures of silica spheres to produce silica-core nanostructure. In addition, SiO_2 sphere nanoparticles also exhibited high stability against coagulation, high reproducibility, chemically inert, water solubility and ability to fine tune the sphere size. These were the key factors making SiO_2 spheres an important materials in biology applications [1,4,5].

Core-shell materials consisted of SiO_2 core and metallic materials shell are attracting considerable attention due to their applications in diverse fields such as biosensors [4], biomedical [6], surface enhanced Raman scattering (SERS) [7], photocatalyses [8] and antibacterial applications [9,10]. This was because of the multifunctional properties of noble metals such as Au, Pt, Ag nanoparticles due to the surface plasmon resonance (SPR). The SPR of metals such as Ag nanoparticles were produced when the incident electromagnetic wave (photon frequency) is in resonance with free conduction electron at the metal surface [11]. Free electron at metal surfaces resulted in strong absorption band of UV–vis spectra at visible range. The sensitivity of Ag nanoparticles toward electromagnetic wave were highly governed by the changes of particle size and packing densities [12,13]. SiO_2-Ag core-shell nanocomposites with rigidly controlled optical properties are potential materials to be applied in biotechnology fields [12,14]. The changes in nanoparticles environment by surrounding biomolecular interactions were detected by the shifting of extinction maximum wavelength in the targeted wavelength range [4].

Generally, the chemical state and elemental analyses of the surface structures can be carried out using X-ray photoelectron spectroscopy (XPS) by studying the binding energy shifts. The chemical state of Ag were reported by many groups. However, these reports were focused only on the peak positioning of Ag binding energy at Ag3d orbital [9,11,15]. The detailed discussion on the binding energies of components O1s was only discussed in mixed perovskite crystal materials as reported by Pawlak et al. [16]. Although Kim et al. [10] and Pan et al. [8] reported the nonsingular O1s orbital binding energy peaks analyses of Ag-SiO_2 nanocomposite, but they did not study comparatively in detail the effect of Ag shell nanoparticles morphologies on binding energy shifts.

At present, a number of reports have been published on the

* Corresponding authors.
E-mail addresses: halina@uniten.edu.my (H. Misran), ramesh79@um.edu.my (S. Ramesh).

https://doi.org/10.1016/j.ceramint.2017.12.118
Received 25 November 2017; Received in revised form 15 December 2017; Accepted 15 December 2017
Available online 16 December 2017

synthesis process and characterizations of core-shell nanocomposite consisting of noble metals nanoparticles (as shell) embedded on sub-micrometer SiO_2 sphere surface (as core) [8,10,11,17]. Methods for synthesizing SiO_2-Ag core-shell nanocomposites, usually involved a bottom-up approach. Typically, bottom-up approach such as wet chemical processing is more facile, using simple instruments and able to produce high amount of yield [8–11]. One of the practical wet chemical processing approach was when using carbon template of surfactants molecules such as polyetheyleneimine (PEI) [18], cetyltrimethyl ammonium bromide (CTAB) [19] and 3-aminopropyltriethoxysilane (APTES) [20] as surface modifier agents. The surface modifier agent was apply on colloidal SiO_2 sphere nanoparticles surface before coating with the respective metal nanoparticles. Nevertheless, these commercial surface modifiers were toxic and expensive [21]. As an approach to introduce cheaper and greener alternative, consequently, straight chain fatty alcohols derived from palm oil (PODFA) was proposed to substitute the commercial surface modifiers [22]. The chemical structure of PODFA consists of a straight hydrocarbon chain with alcohol group (-OH) attached to the terminal carbon. This simple structure compared with conventional surface modifiers makes PODFA a potential substitute materials as alternative surface modifiers for the production of core-shell materials as well as other surface modification uses.

To our knowledge the synthesis of fine Ag nanoparticles coated on SiO_2 sphere by facile and green synthesis method employing PODFA with seeding cycles has not been reported before. PODFA was first introduced as surface modifiers in producing SiO_2-CuO core-shell by our group [22,23]. Furthermore, extensive investigations on the possibilities of PODFA as surface modifier were done on metal coating other than Ag [17]. Therefore, in this paper, we report on the improved non-surfactant surface modification technique by incorporating additional steps of seed mediated approach in order to increase the volume of Ag nanoparticles deposited on the SiO_2 surface to enhance overall surface plasmon properties. Moreover, we focused on studying the chemical shifts and elemental components of Ag, Si and O in SiO_2-Ag core-shell nanocomposites using XPS. The detailed comparative analyses between SiO_2 core and SiO_2-Ag core-shell nanocomposite with different seeding cycles were studied. The results obtained by X-ray diffraction analyses, energy dispersive X-ray and transmission electron microscopy were consolidated to support the presence of core-shell structure. The UV–vis absorbance was used to study the functional materials upon optical stimulus.

2. Experimental procedures

The starting chemicals, tetraethyl orthosilicate ($Si(OC_2H_5)_4$, TEOS, 99%) was obtained from Sigma reagent company. Palm oil derived fatty alcohol (PODFA - decyl-alcohol: C10, 99.7%, Emery Oleochemicals) was used as nonsurfactant surface modifiers in synthesizing SiO_2 spheres and as nonsurfactant surface modifiers in the SiO_2 surface coating process. Ethanol (synthesis grade, J.T. Baker), ammonia water (32% Merck) and silver acetate (98%, Aldrich) were used in the as-–received condition without further purification.

The optimum conditions for synthesizing spherical SiO_2 using nonsurfactant templating method were first reported by Misran et al. [23]. The processes involved in this method were hydrolysis and condensation-polymerization of TEOS in oil-water-alcohol microemulsions mixtures containing nonsurfactant template of PODFA. In a typical experimental procedure, a mixture of water, ethanol, fatty alcohol (C10) and ammonia water were mixed under vigorous stirring. Then, a known volume of TEOS was added drop-wise into the clear microemulsion solution. After several minutes, the white colloidal suspensions were observed. The white suspensions were collected, wash with water and ethanol alternatively several times by centrifugation in order to remove unreacted chemicals and further dried at 373 K overnight.

The synthesis procedure of SiO_2-Ag core-shell nanocomposite was done according to the previous report [22]. Firstly, 0.01 mol% of dried

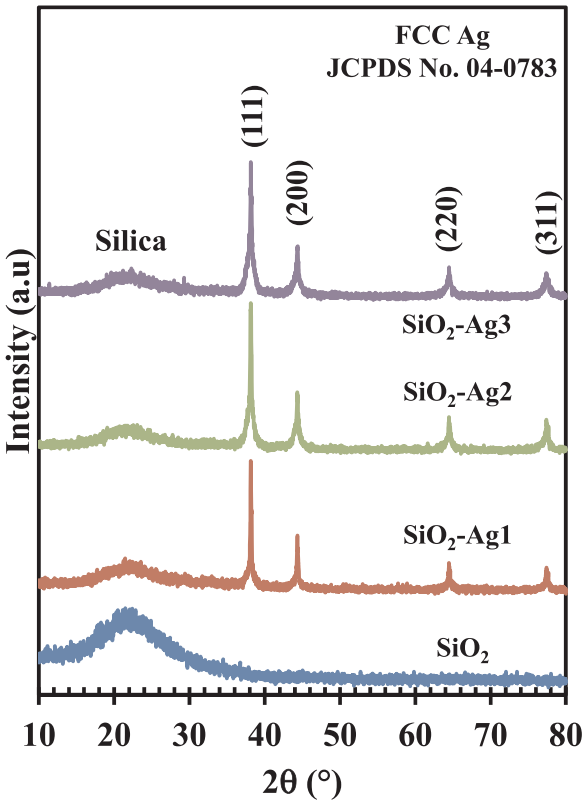

Fig. 1. XRD patterns of calcined SiO_2 and SiO_2-Ag nanocomposites.

SiO_2 spheres were dispersed in ethanol and water using ultrasonification to prepare the SiO_2 sol. Surface modification approach of the silica sol were done by adding PODFA with 10 carbon chain (dodecyl alcohol, C10) and 0.2 ml of 32% ammonia water. Then, the silver acetate precursors were added in three repetition. The mixture was kept constant under stirring at 353 K to complete the seeding reactions. The above procedures were repeated for two and three times in order to increase the number of Ag nanoparticles seed deposited onto the SiO_2 surface. The subsequent suspension were collected and washed with ethanol. Then, the as-synthesized samples were dried at 373 K prior to calcination at 873 K. Obtained SiO_2-Ag core-shell nanocomposite samples were designated as SiO_2-AgX, where X denoted the number of seeding repetitions done.

The phases present in the powder samples were examined at room temperature using X-ray diffractometer (XRD - Shimadzu 6000) at 2θ of 10°–70° with CuK_α radiation (1.50465 Å). The morphology and structure of the Ag shell were studied using transmission electron microscopy (TEM) using FEI G2 F20 at acceleration voltage of 200 kV. Powder samples were dispersed in absolute ethanol, placed and dry on carbon coated copper grid prior to viewing. High-resolution transmission electron microscope (HR-TEM) images were obtained using the same TEM machine (FEI G2 F20) at acceleration voltage of 200 kV. The elemental analyses of prepared samples were carried out using energy dispersive X-ray (EDX) attached with TEM. The acceleration voltage for EDX was at 200 kV. Fourier transform infrared (FT-IR, Perkin Elmer Spotlight 400) prepared with KBr pellets were used to determine the vibration of bonds between atoms in the SiO_2 core and SiO_2-Ag core-shell nanocomposites. X-ray photoelectron spectroscopy (XPS) were conducted using ULVAC-PHI Quantera 11 with a monochromated AlK_α X-ray source ($h\nu$ = 1486.6 eV). XPS was used to determine the chemical identification and chemical state evaluation of the constituent elements. The surface penetration depth was at ca. 6 nm. The XPS was operated at 10^{-7} Pa working pressure in an analysis chamber. The scale of binding energy was referenced to the C 1 s peak at 285.0 eV. The pass

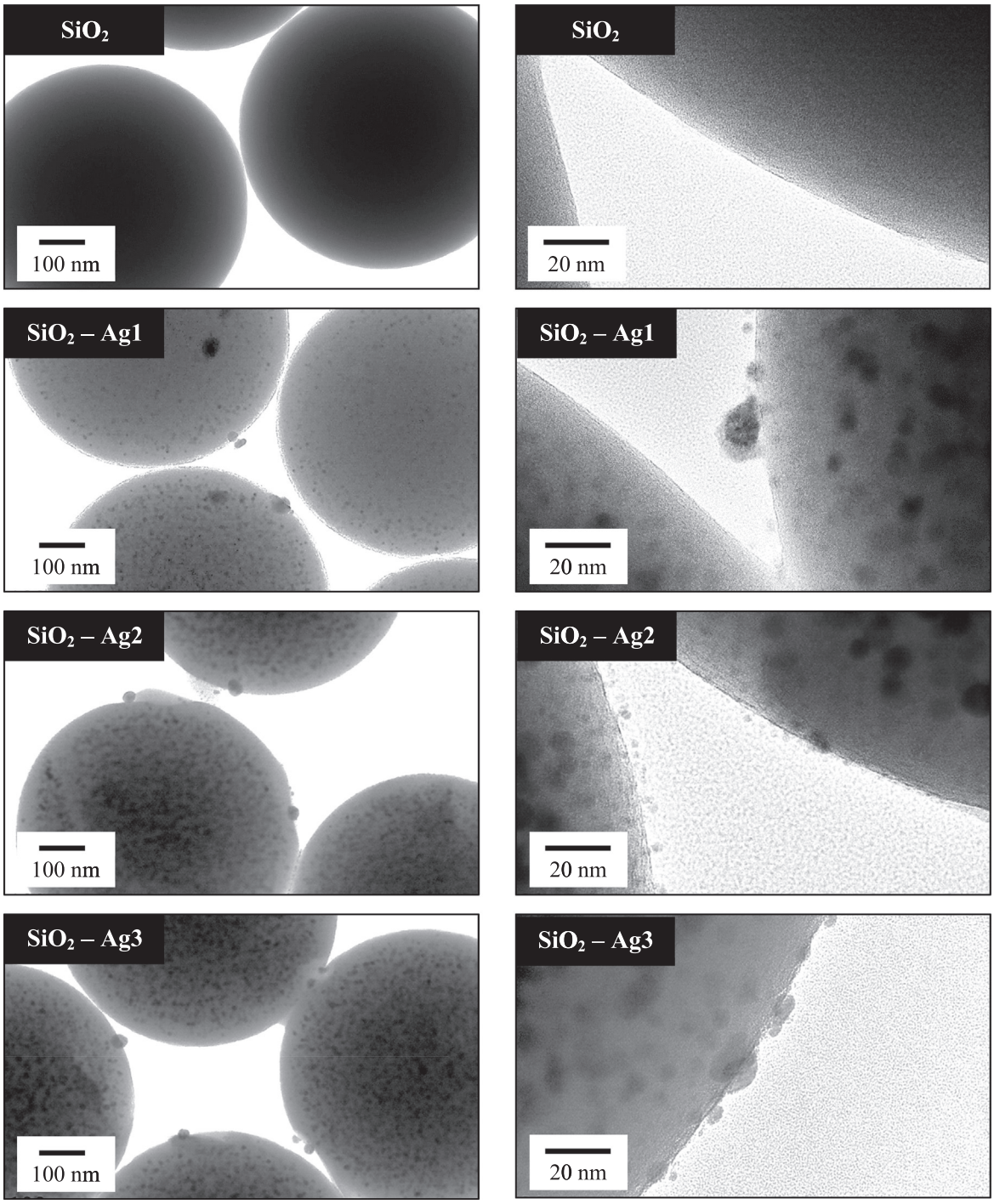

Fig. 2. TEM images of calcined samples SiO_2 and SiO_2-Ag samples taken at various magnifications.

energy of survey scan and narrow scan were used at 280 eV with 1 eV per step and 112 eV with 0.1 eV per step respectively. Data analyses were performed by curve deconvolution using XPS Peak Fitting Program (MultiPack Spectrum). Prior to the deconvolution, charge correction was performed at C 1 s by setting binding energies of C to 284.8 eV. The surface atomic compositions analyses were also done using XPS. The absorption spectra of samples were performed using UV–visible spectrophotometer (Perkin-Elmer Lambda35) equipped with double beam with ethanol baseline.

3. Results and discussion

The XRD patterns of SiO_2 spheres, SiO_2-Ag1, SiO_2-Ag2 and SiO_2-Ag3 core-shell nanocomposites are shown in Fig. 1. The broad XRD reflection peak observed $2\theta = 22^\circ$ is attributable to a typical amorphous structure of silica spheres [23,24]. The broad reflection peaks were also observed in all of core-shell silica samples. There were no other phases found for the silica sample. In contrast, four sharp reflection peaks were detected at $2\theta = 38.14^\circ$, 44.34°, 64.46° and 77.4° for SiO_2-Ag1, SiO_2-Ag2 and SiO_2-Ag3 samples, respectively. These highly crystalline peaks were indexed to (111), (200), (220) and (311) reflection planes of face-centered cubic (FCC) structure of metallic Ag. All of the XRD signatures

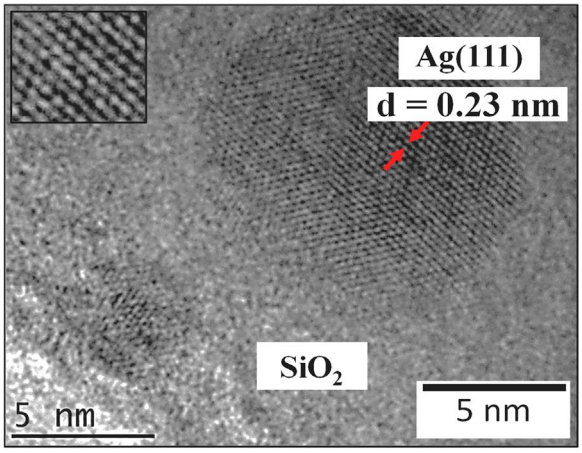

Fig. 3. HRTEM of SiO_2-Ag1 core-shell nanocomposite.

were found to match the reference (JCPDS No. 04–0783). These results were similar to those reported from previous study [17]. The XRD analysis also showed that there was no reaction between SiO_2 and Ag to form an intermetallic phase.

Fig. 2 shows the TEM images of SiO_2 core and SiO_2-Ag samples taken at different magnifications. The prepared SiO_2 spheres exhibited dense and smooth surface texture with diameter of about 450 nm. TEM images of SiO_2-Ag core-shell nanocomposites that had undergone through repeat seeding process of coating with Ag for 1, 2 and 3 times are also presented in Fig. 2. The TEM images showed sphere-like Ag nanoparticles, having varying diameters from 5 to 20 nm deposited in scattered area on the smooth SiO_2 surface. The Ag nanoparticles were more closely packed to each other for samples SiO_2-Ag2 and SiO_2-Ag3 which were prepared with two and three times of repeat seeding process, respectively. These results suggested that seeding process with more than one repetition played an important role in enhancing the volume of deposited Ag nanoparticles onto the core materials to produce core-shell nanocomposites.

The representative HRTEM of SiO_2-Ag1 sample is shown in Fig. 3 with a low-resolution image (inset) taken at Ag nanoparticle area. The structure of SiO_2-Ag core-shell nanocomposites consisted of dense silica spheres structure and the observed interplanar *d*-spacing of (111) plane was at about 0.23 nm. The lighter area suggested structure of SiO_2 core material and black spot nanoparticles at ca. 10 nm size belongs to the Ag crystallites which was deposited on the SiO_2 surface. This was because the Ag nanoparticle on SiO_2 surface has a FCC arrangement with observed interplanar *d*-spacing value which is very close to the value of (111) lattice planes obtained from the XRD data at ca. 0.2361 nm. These results coincided well with a cubic lattice of Ag obtained from JCPDS No.: 04–0783 [17].

The elemental analysis results obtained from EDX and XPS analyses of SiO_2 core and SiO_2-Ag core-shell samples are listed in Table 1. The corresponding EDX spectra are shown in Fig. 4. The results showed the present of Ag element in all SiO_2-Ag core-shell with various cycles of seeding process and the absent of Ag element in the SiO_2 sample. The atomic percentage of Ag element and Ag3d orbital increased from SiO_2-Ag1 prepared with one seeding cycle to SiO_2-Ag3 prepared with three seeding cycles. These results suggested that the number of seed repetitions was the reason for the increment in the amount of Ag nanoparticles deposited onto SiO_2 surfaces. The presence of C and Cu as shown in Fig. 4 can be attributed to the sample grid used for the analysis.

The FT-IR spectrum was used to identify the vibration characteristics of atomic bonding between Si, O, H and Ag. The FT-IR spectra of SiO_2 core and SiO_2-Ag core-shell nanocomposites are shown in Fig. 5. The FT-IR spectrum of SiO_2 core exhibited the absorption bands from stretching vibration of O-H (ν_{stret} at ca. 810 cm^{-1}), asymmetric vibration of Si-O-H (ν_{assym} at ca. 960 cm^{-1}), symmetric vibration of Si-O-Si (ν_{sym} at ca. 1130 cm^{-1}), stretching vibration of C=C (ν_{stret} at ca. 1630 cm^{-1}) and stretching vibration of O-H (ν_{stret} at ca. 3000 cm^{-1} to 3700 cm^{-1}). These absorption bands were in good agreement with FT-IR analyses obtained from Misran et al. [23]. The absorption peaks of SiO_2 core spectrum were similar to the absorption peaks observed in SiO_2-Ag spectrum. However, the significant absorption peak of asymmetric stretching vibration originating from ν_{assym} Si-O-H (silanol) at ca. 960 cm^{-1} was not seen in SiO_2-Ag core-shell nanocomposite spectrum suggesting that the silanols formed bond with the deposited Ag nanoparticles. In addition, the broad shoulder peak observed in SiO_2 core spectrum at ca. 3774 cm^{-1} attributable to the isolated silanols were not observed in SiO_2-Ag core-shell nanocomposite spectrum [23]. These results suggested that the silanols bond was broken due to calcination process of SiO_2-Ag core-shell nanocomposite sample. It was also suggested that Si atom from silanol group was bonded with Ag atom to form Si-O-Ag bond that could not be detected in FT-IR analyses but possible to be observed in XPS analyses. The broad absorption band of SiO_2 core spectrum observed at ca. 3300 cm^1 – 3700 cm^{-1} region may be attributed to the overlapping of hydrogen bond in OH group including H-bonded with H_2O, alcohol, terminal hydroxyl and Si–OH in carbon chain [23,25]. Furthermore, based on the surface chemistry studies of amorphous SiO_2 reported by Zhuravlev [5], the material has surface properties containing OH group. However the broad absorption band at ca. 3300 cm^{-1} – 3700 cm^{-1} region exhibited narrow and low intensity for the SiO_2-Ag core-shell nanocomposite spectrum. These results suggested that the volume of OH stretching vibrations in H-bonded water were reduced. The reduction was due to the elimination of absorbed water during calcination process in order to obtained SiO_2-Ag core-shell nanocomposite. The incorporation of Ag into SiO_2 surface also contributed to the decrement of absorption peak at ca. 3300 cm^{-1} – 3700 cm^{-1} region.

XPS spectra were obtained in order to elucidate both the elemental components and chemical state of the elements of SiO_2 core and SiO_2-Ag core-shell nanocomposite samples. Fig. 6 shows the survey scan spectrum of SiO_2 core and survey scan spectra of SiO_2-Ag samples. New peaks at ca. 370 eV attributable to Ag3d binding energy and 573 eV attributable to Ag3p3 binding energy were observed significantly in SiO_2-Ag spectra suggesting the presence of Ag in the sample. The narrow scan XPS spectra of Si2p, Ag3d and O1s spectra of prepared

Table 1
Elemental analysis of SiO_2 and SiO_2-Ag core-shell nanocomposites.

Material	EDX analysis										XPS analysis			
	atomic %					weight %					atomic %			
	Ag	Si	O	C	Cu	Ag	Si	O	C	Cu	C1s	O1s	Si2p	Ag3d
SiO_2	–	33.93	51.5	13.11	1.44	–	47.03	40.66	7.77	4.53	0.55	69.83	29.62	–
SiO_2-Ag1	1.27	29.8	55.6	11.87	1.44	6.56	39.88	42.39	6.79	4.37	0.91	69.47	29.02	0.6
SiO_2-Ag2	2.02	28.66	47.37	13.20	8.72	8.76	32.26	30.38	6.35	22.23	1.57	68.90	28.82	0.72
SiO_2-Ag3	2.66	32.86	50.66	9.79	4.0	11.99	38.57	33.87	4.91	10.64	1.08	68.40	29.06	1.45

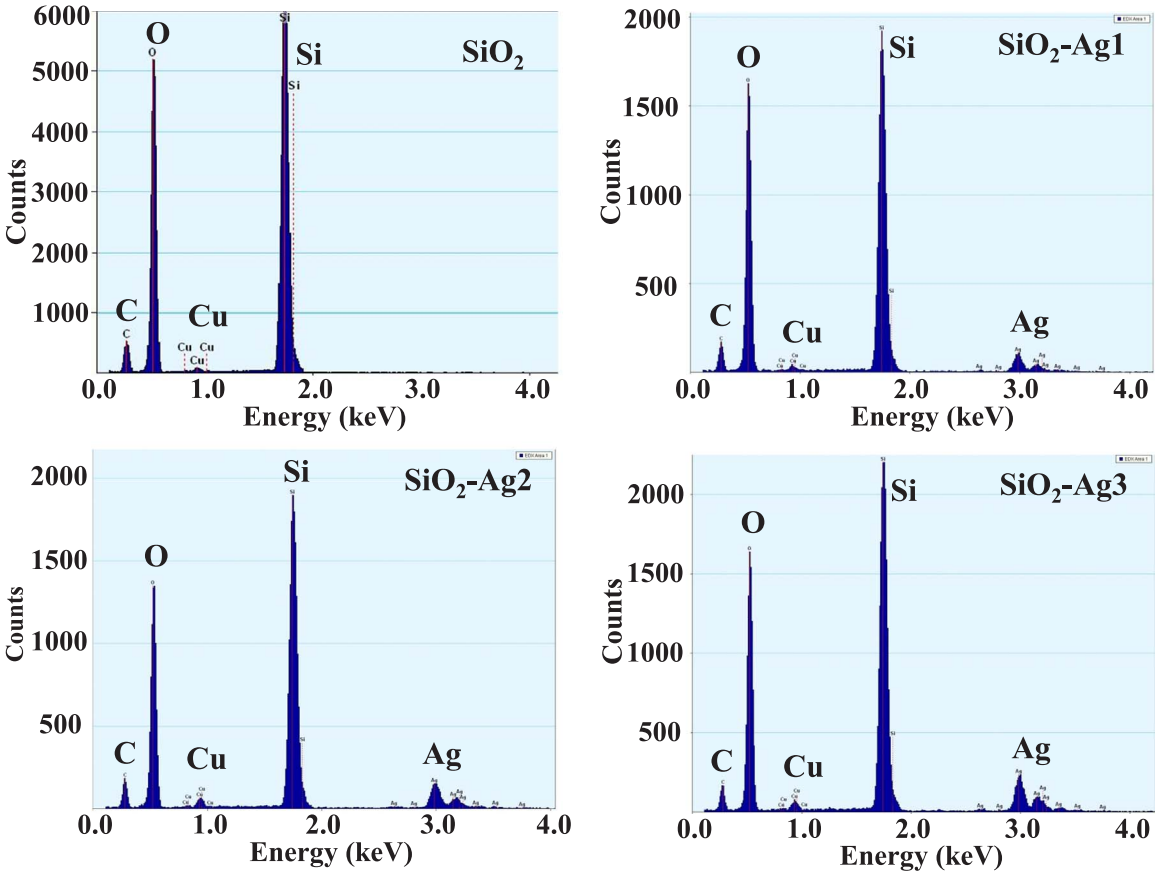

Fig. 4. EDX spectra of calcined SiO_2 and SiO_2-Ag core-shell nanocomposites.

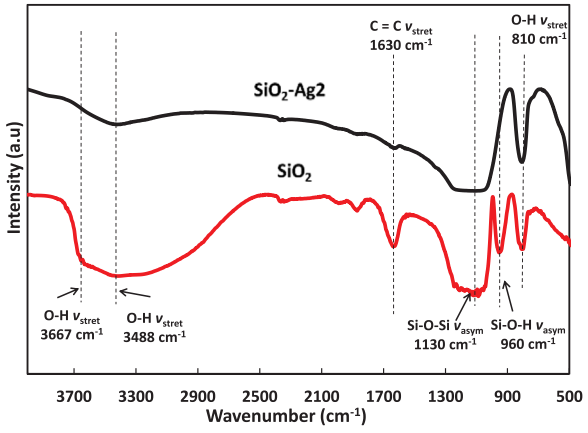

Fig. 5. FT-IR spectra of SiO_2 core and SiO_2-Ag with 2 times seed recrystallization.

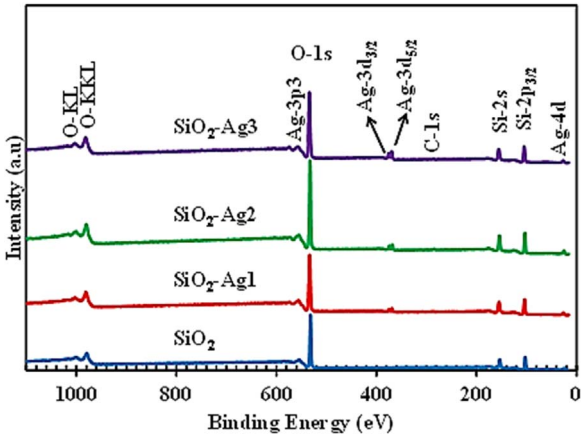

Fig. 6. XPS survey scan for Si2p, Ag3d and O1s of prepared samples.

samples are shown in Fig. 7, Fig. 8 and Fig. 9, respectively. Curve fitting or deconvolution was done at the obtained XPS signals to identify the possibility of unknown binding energy.

The binding energy peak of SiO_2 core at ca. 103.4 eV as shown in Fig. 7 was attributed to the Si-O core electron. The value obtained in this study was very close to the literature value [10,26,27]. The position of peak for SiO_2-Ag samples suggested slight shift towards higher binding energy state at ca. 103.6 eV. This could be attributed to the interaction between Si-O groups of SiO_2 surface framework with Ag nanoparticles.

The narrow scan spectra of Ag3d peaks for SiO_2-Ag1, SiO_2-Ag2 and SiO_2-Ag3 nanocomposites are shown in Fig. 8, exhibiting the spin orbit components of $3d_{5/2}$ and $3d_{3/2}$. Both peaks of $Ag3d_{5/2}$ and $Ag3d_{3/2}$ were well deconvoluted by two components consisting of zero-valence (Ag°) and mono-valence (Ag^{+}) attributable to the pure Ag and Ag bonded with other atom respectively. There are two possible bonding between Ag^{+} with other atoms, namely; 1) Ag_2O nanoparticles and 2) Si-O-Ag linkages which were Ag^{+} bonded with $Si\text{-}O^{-}$ from SiO_2 surfaces. However, XRD analyses (Fig. 1) did not exhibit any diffraction peaks corresponding to Ag_2O phases. Thus, this result suggested that the deconvoluted peaks of Ag^{+} could be assigned to the Si-O-Ag binding energy occurring on the surface of the samples. Meanwhile, XPS is a surface analytical technique in which the penetration depth is at ca. 6 nm. The binding energies of Ag° for $Ag3d_{5/2}$ orbit were at ca. 368.7 eV and for $Ag3d_{3/2}$ orbit were at ca. 374.7 eV. On the other hand, the binding energies of Ag^{+} for $Ag3d_{5/2}$ orbit and $Ag3d_{3/2}$ orbit were at ca. 367.9 eV and 373.9 eV, respectively. These results were in good agreement with that reported by other researchers [8,28]. The wide

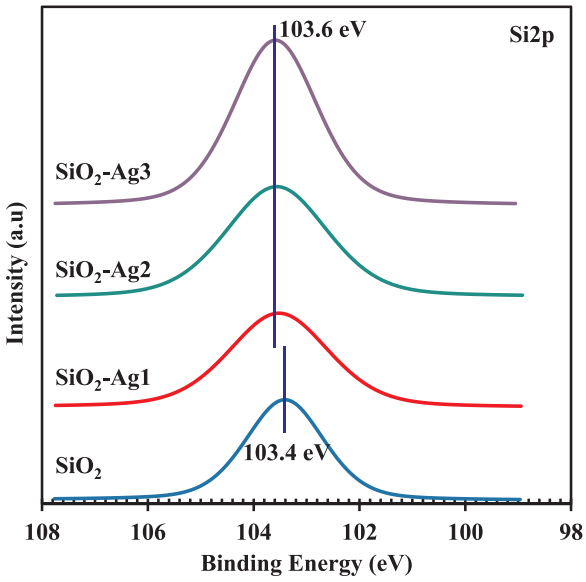

Fig. 7. XPS narrow scan for Si2p orbit of prepared samples.

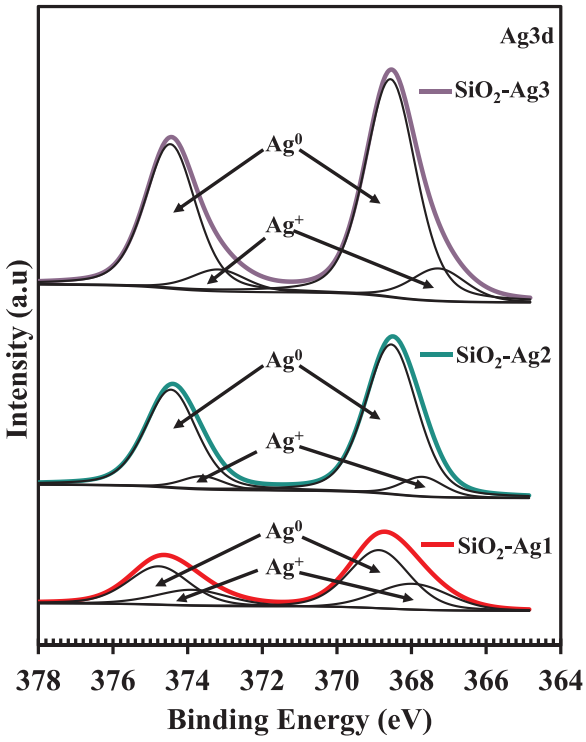

Fig. 8. XPS narrow scan at Ag3d orbit of prepared samples.

area under the deconvoluted XPS spectra as shown in Fig. 8 demonstrated high amount of Ag nanoparticles presence on the silica core surface. In Fig. 8, the bold curve represents Si-O-Ag while non-bold line represents pure metallic Ag. From the deconvoluted peaks observation, the amount of metallic Ag on the SiO_2 sphere surface increased with the increased in number of seeding cycles. These results suggested that the number of seed repetition directly affected the amount of Ag nanoparticles formed on the silica core.

The deconvoluted O1s core level spectra are shown in Fig. 9. These spectra were resolved into two oxides components for SiO_2 core spectrum and three oxides components for SiO_2-Ag core-shell nanocomposite samples after curve fitting. The components were Si-O-H and Si-O-Si in SiO_2 core spectrum and additional peak of Si-O-Ag in SiO_2-Ag

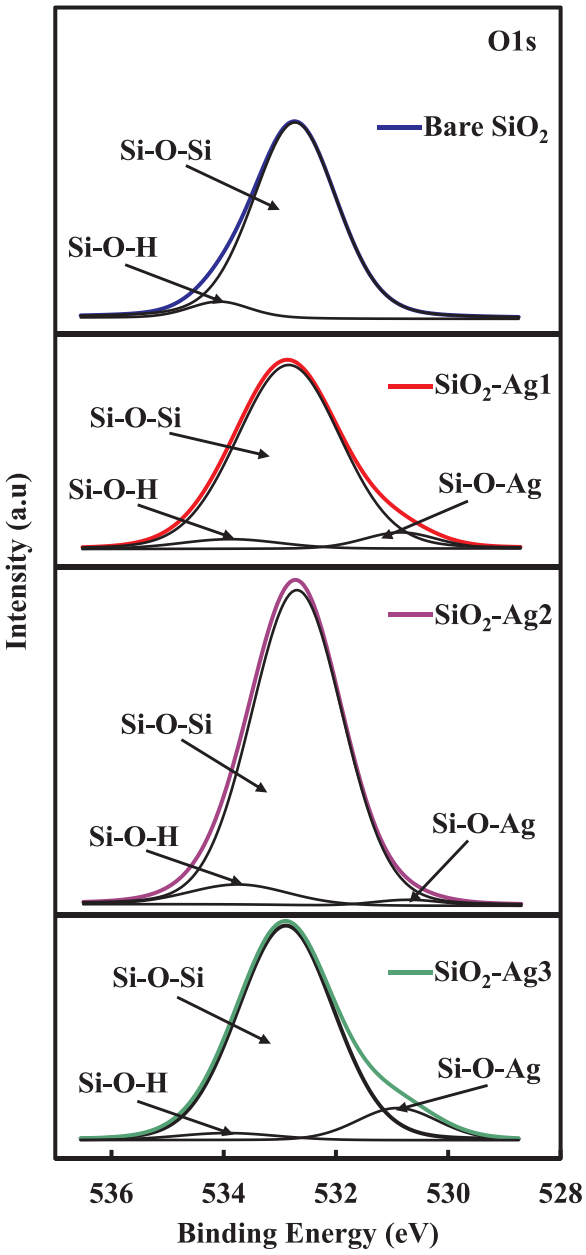

Fig. 9. XPS narrow scan at O1s orbit of prepared samples.

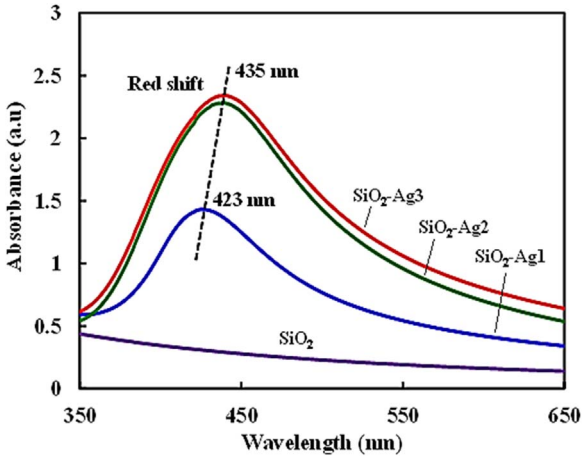

Fig. 10. UV–vis absorption spectra of SiO_2 and SiO_2-Ag nanocomposites.

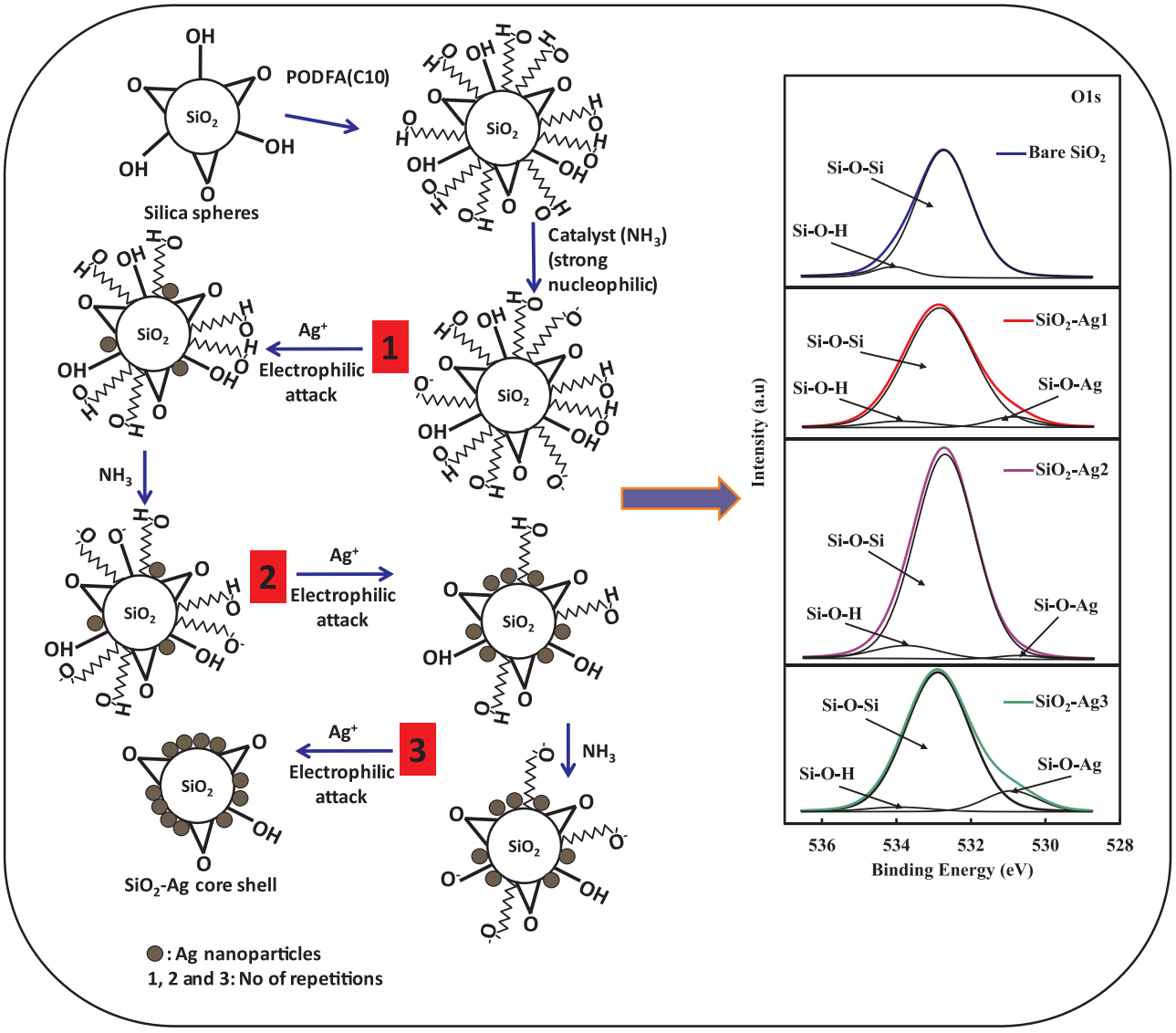

Fig. 11. Schematic illustration of the surface modification mechanism of SiO_2-Ag core-shell.

spectra. The binding energies of O1s were observed at ca. 533.8 eV for Si-O-H, ca. 532.8 eV for Si-O-Si and ca. 530.8 eV for Si-O-Ag. These results coincided well with the values obtained in previous reports [10,29]. The position of corresponding binding energy peaks of those three oxides were assigned based on ionic character and electronegativity of atom in molecule. The ionic character between H atom in Si-O-H and Si in Si-O-Si were taken into account in order to identify the position of Si-O-H and Si-O-Si. According to Pawlak et al.[16], the more ionic the bonding, the binding energy value will be shifted towards lower binding energy. The Si-O-Si bonding was having ionic characteristics as compared to Si-O-H bonding. This would make Si atoms easier to receive the core electron from O in Si-O-Si. On the other hand, in Si-O-H the bonding characteristics would give the opposite effect with H atom making it difficult to receive the core electron from O in Si-O-H. Consequently, it is easier to eject the electron from O core level in Si-O-Si than from Si-O-H, resulting in lower binding energy signal in Si-O-Si than in Si-O-H. In the case of positioning between Si-O-Ag and Si-O-Si bonding, the rules of electronegativity were used. The electronegativity values of Ag and Si were at ca. 1.9 and 1.8 respectively [30]. The high electronegativity of an atom means more easier for the atom in a molecule to attract electron towards itself. Therefore, the valence electron density of O in Si-O-Ag will be moved towards Ag greater than O in Si-O-Si toward Si. This phenomenon made it easier to eject the electron from O core level in Si-O-Ag than from O core level in Si-O-Si. Thus, the binding energy of O1s in Si-O-Ag was observed at lower binding energy if compared to O1s in Si-O-Si.

UV–visible analyses were performed to confirm the formation of Ag nanoparticles on SiO_2 core surfaces and to elucidate the optical responses of SiO_2-Ag core-shell nanocomposite. The optical absorption spectra of SiO_2 core and SiO_2-Ag core-shell nanocomposite are shown in Fig. 10. The absorption spectrum of SiO_2 core was used as reference. It can be seen that no absorption peak was presence in SiO_2 core spectrum. In contrast, broad absorption peak appeared at ca. 423 nm for the SiO_2-Ag1 sample. However, the peak intensity was higher, broader and shifted towards higher wavelength at ca. 435 nm for SiO_2-Ag2 and SiO_2-Ag3 samples. All three absorption peaks were observed in the visible range of the electromagnetic spectra. This absorption peak was known as surface plasmon resonance due to the resonance between collective oscillations of conduction electron on the metal nanoparticles surfaces with incident electromagnetic radiation. On the other hand, shifting of position for surface plasmon resonance was known as the red shift [12,31]. It was reported that the position and intensity of surface plasmon absorption for Ag nanoparticles were influenced by particle size, particle shape, state of aggregation and surrounding medium [11,12,31].

Based on the results obtained, a surface modification mechanism of

the SiO_2-Ag core-shell has been proposed as shown in Fig. 11. As the number of seeding repetitions increased, the intensity of absorption peak became higher and broader. This was due to the amount of Ag nanoparticles that increased on the SiO_2 surface as the seeding repetitions increased [13]. The results coincided well with the elemental analyses obtained from EDX and XPS (see Table 1). The absorption peak exhibited red-shift from ca. 423 nm for SiO_2-Ag1 to ca. 435 nm for SiO_2-Ag3 and this can be attributed to the increased in the volume of the Ag nanoparticles seeding on SiO_2 surface as shown in Fig. 2. This would facilitate the interaction between neighbouring Ag nanoparticles, thus promoting red shift and broadening of plasmon peaks. The SiO_2-Ag core-shell nanocomposite obtained in this study showed great sensitivity to morphology changes. These results suggested that core-shell nanocomposites can be a better choice for optical biosensor, optoelectronic and therapeutic applications [4,6–8].

4. Conclusions

SiO_2-Ag core-shell nanocomposites were successfully prepared using nonsurfactant sol-gel surface modification method. Seed mediated techniques were used in order to increase the volume of Ag nanoparticles deposited on the SiO_2 surfaces. The binding energies of Si-O-Ag, Si-O-Si and Si-O-H were determined at ca. 530.8 eV, 532.8 eV and 533.8 eV, respectively. The number of seed repetitions highly affected the morphology and elemental analyses of SiO_2-Ag core-shell nanocomposite samples and thus affected the optical absorption. The volume of Ag element and Ag3d orbital increased with the increasing number of seeding repetitions. Surface plasmon resonance peaks were moved to a red-shift with increased intensity due to higher volume of Ag nanoparticles deposited on to silica core. This work showed that the optical properties could be changed by controlling the volume of Ag nanoparticles. From the optical response results, SiO_2-Ag core-shell nanocomposite obtained in this study exhibited favourable properties to be applied as optical biosensors, optoelectronics and therapeutic applications.

Acknowledgements

The authors thank Ministry of Higher Education (MOHE) under FRGS schemes (Grant number: FRGS20130106 and FRGS20150116).

References

[1] B.J. Jankiewicz, D. Jamiola, J. Choma, M. Jaroniec, Silica-metal core-shell nanostructure, Adv. Colloid Interface Sci. 170 (2012) 28–47.
[2] R. Subasri, R. Malathi, A. Jyothirmayi, N.Y. Hebalkar, Synthesis and characterization of CuO-hybrid silica nanocomposite coatings on SS 304, Ceram. Int. 38 (2012) 5731–5740.
[3] Y. Zhu, H. Da, X. Yang, Y. Hu, Preparation and characterization of core–shell monodispersed magnetic silica microspheres, Colloids Surf. A: Physicochem. Eng. Asp. 231 (2003) 123–129.
[4] S.A. Kalele, R. Dey, N. Hebalkar, J. Urban, S.W. Gosavi, S.K. Kulkarni, Synthesis and characterization of silica-titania core-shell particles, Pramana-J. Phys. 65 (2005) 787–791.
[5] L.T. Zhuravlev, The surface chemistry of amorphous silica. Zhuravlev model, Colloids Surf. A: Physicochem. Eng. Asp. 173 (2000) 1–38.
[6] B.N. Khlebtsov, N.G. Khlebtsov, Biosensing potential of silica/gold nanoshells: sensitivity of plasmon resonance to the local dielectric environment, J. Quant. Spectrosc. Radiat. Transf. 106 (2007) 154–169.
[7] T. Liu, D. Li, D. Yang, M. Jiang, An improved seed-mediated growth method to coat complete silver shells onto silica spheres for surface-enhanced Raman scattering, Colloids Surf. A: Physicochem. Eng. Asp. 387 (2011) 17–22.
[8] K.Y. Pan, Y.F. Liang, Y.C. Pu, Y.J. Hsu, J.W. Yeh, H.C. Shih, Studies on the photocatalysis of core-shelled SiO_2–Ag nanospheres by controlled surface plasmon resonance under visible light, Appl. Surf. Sci. 311 (2014) 399–404.
[9] K. Nischala, T.N. Rao, N. Hebalkar, Silica–silver core–shell particles for antibacterial textile application, Colloids Surf. B: Biointerfaces 82 (2011) 203–208.
[10] Y.H. Kim, D.K. Lee, H.G. Cha, C.W. Kim, Y.S. Kang, Synthesis and characterization of antibacterial Ag–SiO_2 nanocomposites, J. Phys. Chem. C 111 (2007) 3629–3635.
[11] V.G. Pol, D.N. Srivastava, O. Palchik, V. Palchik, M.A. Slifkin, A.M. Weiss, A. Gedanken, Sonochemical deposition of silver nanoparticles on silica spheres, Langmuir 18 (2002) 3352–3357.
[12] L. Mahmudin, E. Suharyadi, A.B.S. Utomo, K. Abraha, Optical properties of silver nanoparticles for surface plasmon resonance (SPR)-based biosensor applications, J. Mod. Phys. 6 (2015) 1071–1076.
[13] Z. Chen, X. Chen, L. Zheng, T. Gang, T. Cui, K. Zhang, B. Yang, A simple and controlled method of preparing uniform Ag midnanoparticles on Tollens-soaked silica spheres, J. Colloid Interface Sci. 285 (2005) 146–151.
[14] D.A. Stuart, A.J. Haes, C.R. Yonzon, E.M. Hicks, R.P.V. Duyne, Biological applications of localised surface plasmonic phenomenae, IEEE Proc. Nanobiotechnol. 152–1 (2005) 13–32.
[15] E. Sumesh, M.S. Bootharaju, Anshup, T. Pradeep, A practical silver nanoparticle-based adsorbent for the removal of Hg2 + from water, J. Hazard. Mater. 189 (2011) 450–457.
[16] D.A. Pawlak, M. Ito, M. Oku, K. Shimamura, T. Fukuda, Interpretation of XPS O (1s) in mixed oxides, proved on the mixed perovskite crystals, J. Phys. Chem. B 106 (2002) 504–507.
[17] M.A. Salim, H. Misran, S.Z. Othman, N. Mahadi, N.I.M. Pauzi, A. Manap, Synthesis and characterizations of SiO_2-Ag core-shell nanostructure using fatty alcohols as surface modifiers, Appl. Mech. Mater. 773–774 (2015) 199–203.
[18] J. Xue, C. Wang, Z. Ma, A facile method to prepare a series of SiO_2@Au core/shell structured nanoparticles, Mater. Chem. Phys. 105 (2007) 419–425.
[19] J.H. Park, S.G. Oh, Facile synthesis of silica–manganese oxide nanocomposites with core–shell structure using surfactant and cosurfactant, Colloids Surf. A: Physicochem. Eng. Asp. 390 (2011) 199–206.
[20] S.N. Abdollahi, M. Naderi, G. Amaobediny, Synthesis and physicochemical characterization of tunable silica–gold nanoshells via seed growth method, Colloids Surf. A: Physicochem. Eng. Asp. 414 (2012) 345–351.
[21] W. Tian, J. Yao, R. Liu, M. Zhu, F. Wang, X. Wu, H. Liu, Effect of natural and synthetic surfactants on crude oil biodegradation by indigenous strains, Ecotoxicol. Environ. Saf. 129 (2016) 171–179.
[22] M.A. Salim, H. Misran, S.Z. Othman, N.N.H. Shah, N.A.A. Razak, A. Manap, Effect of NH_3 on structural and optical properties of SiO_2-CuO core-shell nanostructure, Appl. Mech. Mater. 465–466 (2014) 813–818.
[23] H. Misran, M.A. Yarmo, S. Ramesh, Synthesis and characterization of silica nanospheres using nonsurfactant template, Ceram. Int. 39 (2013) 931–940.
[24] H. Misran, S. Ramesh, M.J. Ghazali, Palm oil based fatty alcohols templated mesoporous silica and silica spheres, Int. J. Nanosci. 10 (2011) 1275–1281.
[25] M. Mizukami, Y. Nakagawa, K. Kurihara, Surface induced hydrogen-bonded macrocluster formation of methanol on silica surfaces, Langmuir 21 (2005) 9402–9405.
[26] D.K. Sarkar, S. Dhara, K.G.M. Nair, S. Chowdhury, Studies of phase formation and chemical states of the ion beam mixed Ag/Si(111) system, Nucl. Instrum. Methods Phys. Res. B 168 (2000) 215–220.
[27] Q. Chen, W. Shi, Y. Xu, D. Wu, Y. Sun, Visible-light-responsive Ag–Si codoped anatase TiO_2 photocatalyst with enhanced thermal stability, Mater. Chem. Phys. 125 (2011) 825–832.
[28] P. Prieto, V. Nistor, K. Nouneh, M. Oyama, M.A. Lefdil, R. Díaz, XPS study of silver, nickel and bimetallic silver–nickel nanoparticles prepared by seed-mediated growth, Appl. Surf. Sci. 258 (2012) 8807–8813.
[29] Y. Sohn, SiO_2 nanospheres modified by Ag nanoparticles: surface charging and CO oxidation activity, J. Mol. Catal. A: Chem. 379 (2013) 59–67.
[30] W.F. Smith, J. Hashemi, Foundations of Materials Science and Engineering, McGraw-Hill, United Kingdom, 2003, pp. 119–124.
[31] J. Kang, Y. Li, Y. Chen, A. Wang, B. Yue, Y. Qu, Y. Zhao, H. Chu, Core–shell Ag@SiO_2 nanoparticles of different silica shell thicknesses: preparation and their effects on photoluminescence of lanthanide complexes, Mater. Res. Bull. 71 (2015) 116–121.